Electronic Supplementary Material

Tuning a consistent near-infrared photo-initiated multimodal tumor strategy based on the core-shell structure of gold star@PB@CuS nanoparticles

Yao Zhong[a], XiaoLei Li[b], Li Ye[a], Pengcheng Zhu[a], Lin Zhuang [a*]

[a] *School of Physics, State Key Laboratory of Optoelectronic Materials and Technologies, Guangdong Provincial Key Laboratory of Photovoltaics Technologies, Sun Yat-sen University, Guang zhou 510006, People's Republic of China*

[b] *Department of Orthodontics, School of Dental Medicine at University of Pennsylvania, Philadelphia, PA, 19104, USA*

*Corresponding author. E-mail address: stszhl@mail.sysu.edu.cn

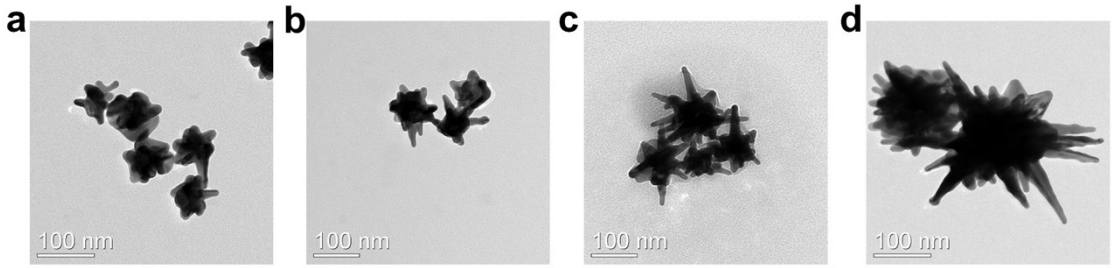

Figure S1. Transmission electron microscope (TEM) images of Au nanostars synthesized with different seed concentrations (a) 1000 μL (b) 800 μL (c) 600 μL (d) 100 μL.

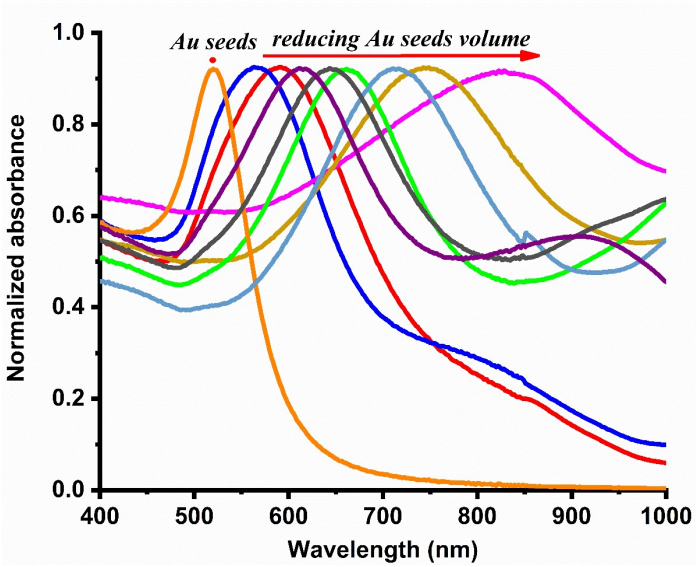

Figure S2. The absorption spectrum of gold nanostars varies as the volume of added gold seeds gradually decreases.

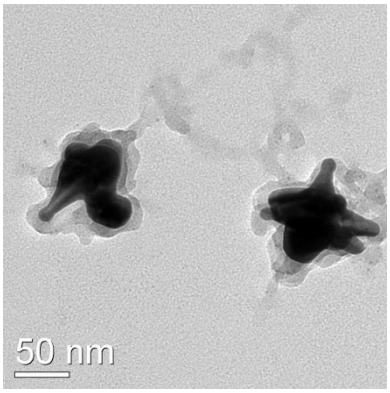

Figure S3. Gold star@PB NPs synthesized using dilute concentration of PB.

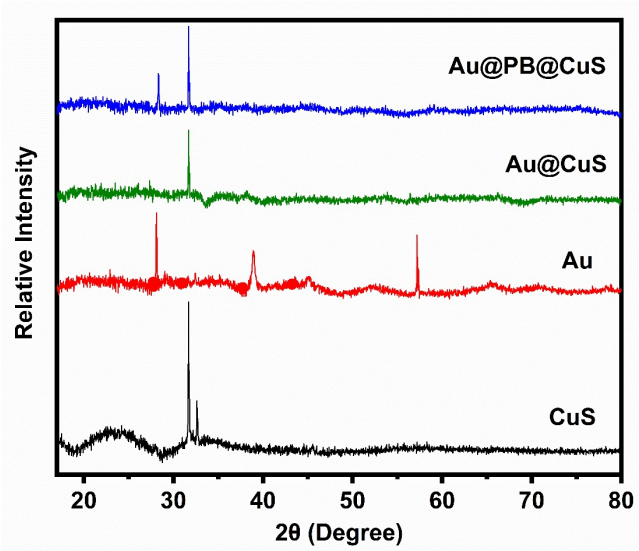

Figure S4. X-ray diffraction (XRD) patterns of GPC and each component.

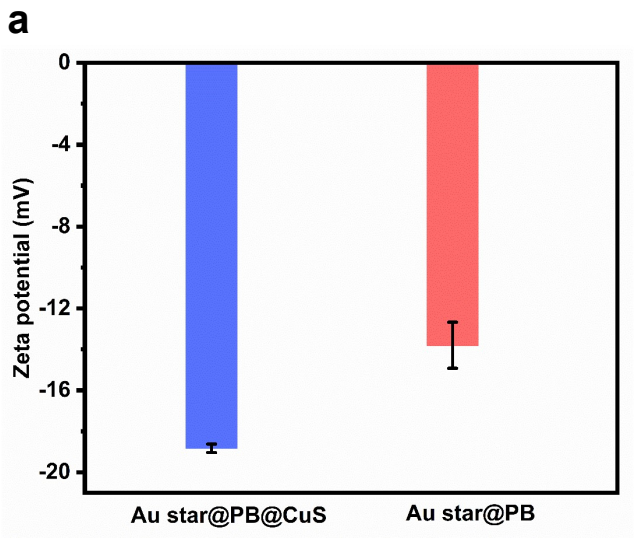

Figure S5a. ζ-potential diagrams of Au star@PB@CuS (GPC) and Au star@PB.

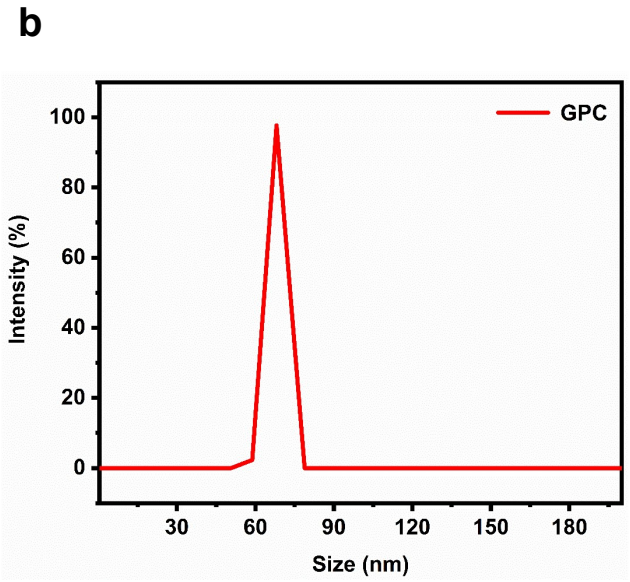

Figure S5b. The dynamic light scattering size of the GPC.

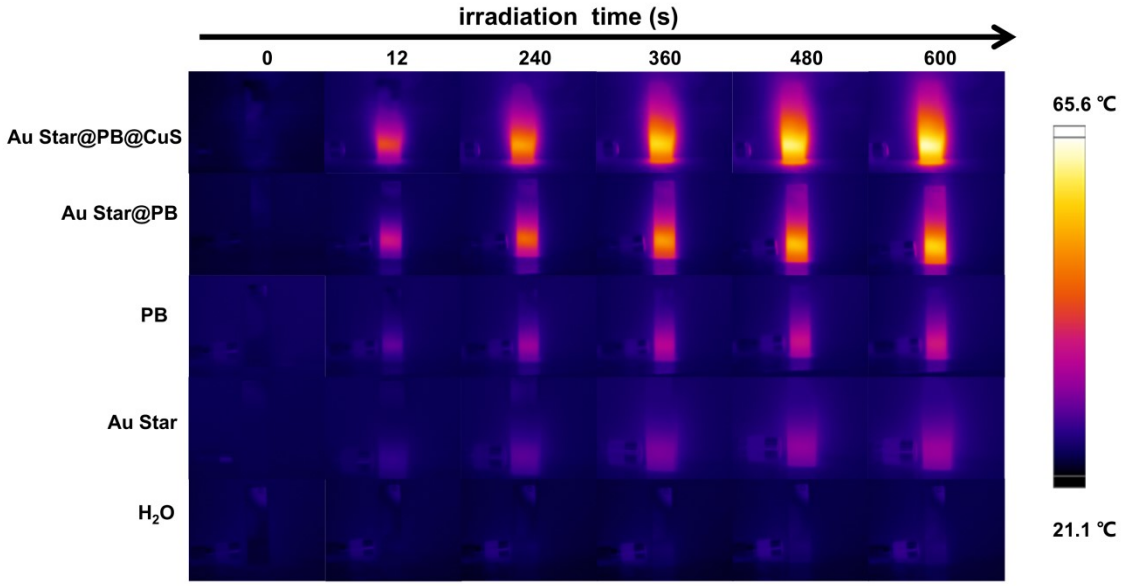

Figure S6. NIR photothermal images of the Control group and GPC and each component under the laser irradiation (808 nm, 1W/cm^2).

a

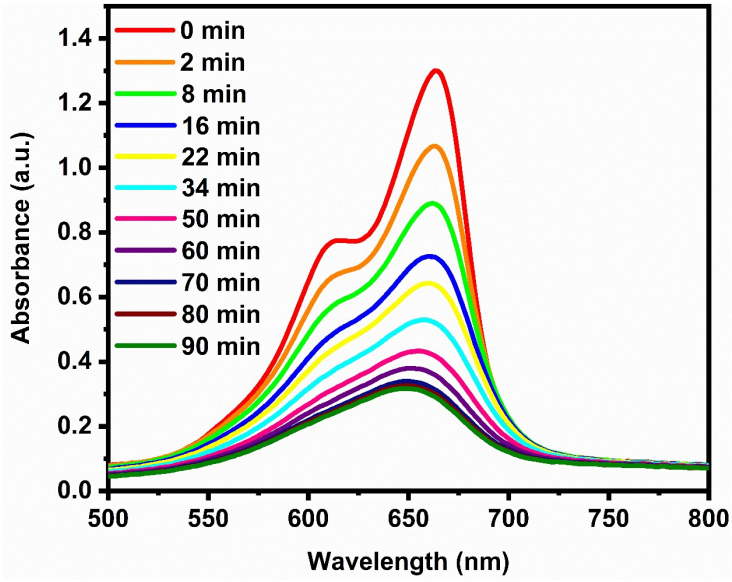

Figure S7a. The degradation process of MB was incubated with GPC+H_2O_2+GSH solution for different times (0-90 min).

b

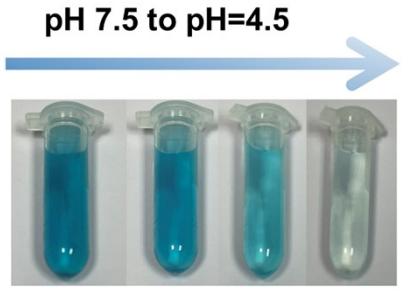

Figure S7b. The degradation of MB solution in the range of pH=7.5 to pH=4.5 after 30 min was observed following the addition of GPC+H_2O_2+GSH.

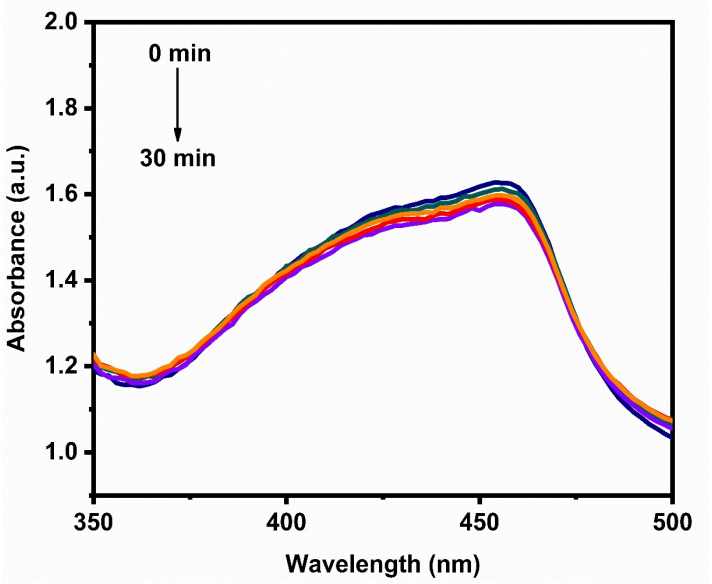

Figure S8. Degradation of DPBF in the absence of laser irradiation.

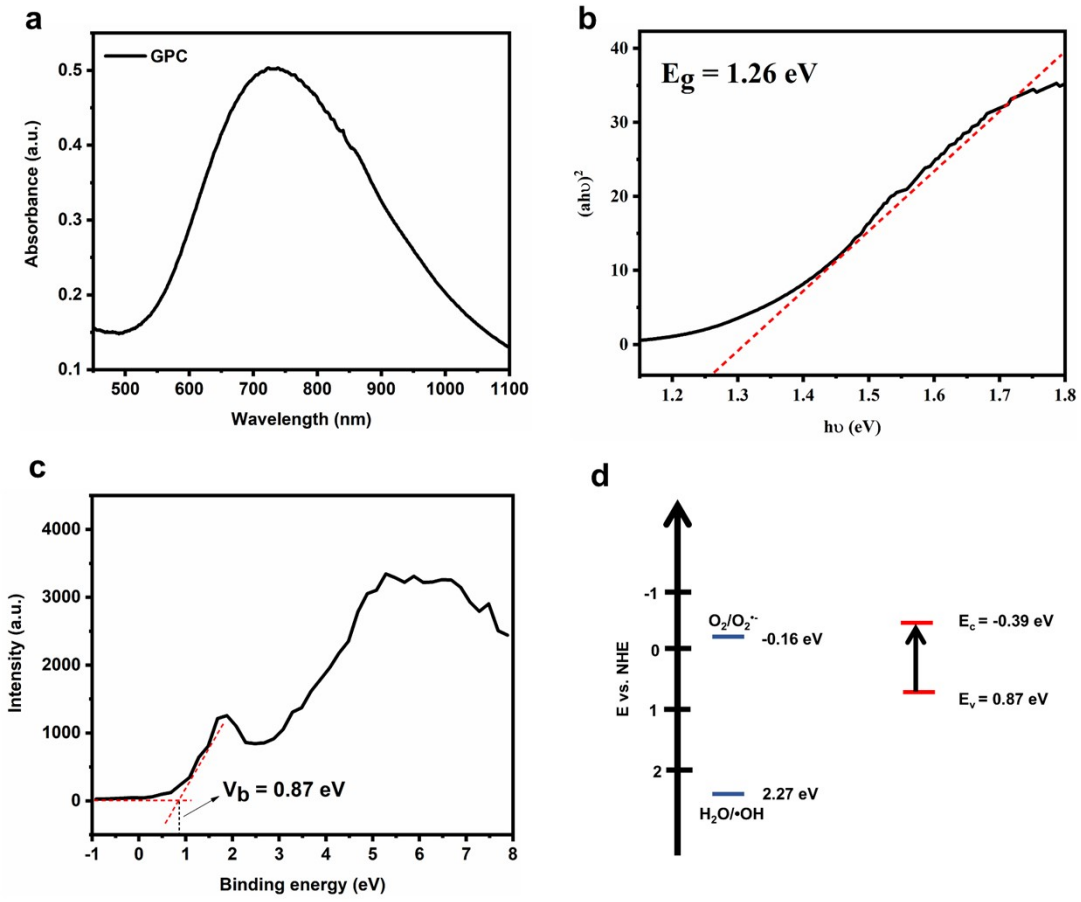

Figure S9. (a) The UV-Vis absorbance spectrum of GPC. (b) Plots of $(ah\nu)^2$ and photon energy ($h\nu$) for the band gap energy. (c) The XPS spectrum of GPC valence band (VB). (d) Mechanism of $O_2^{\bullet-}$ generation by GPC under an 808 nm laser irradiation.

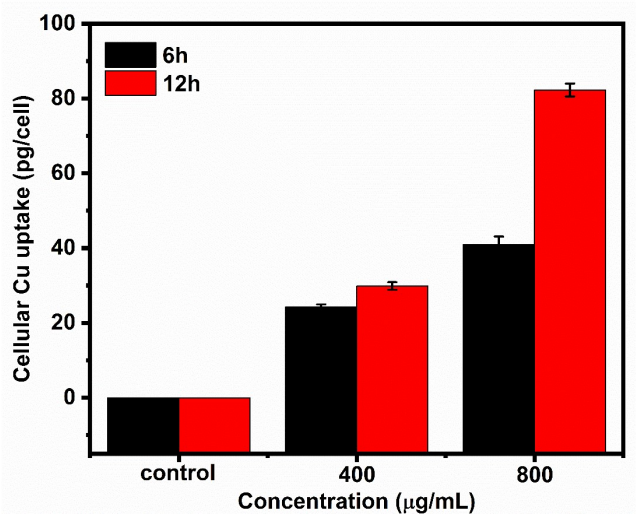

Figure S10. The Cu uptake by 4T1 cells treated with GPC for 6 or 12 h.

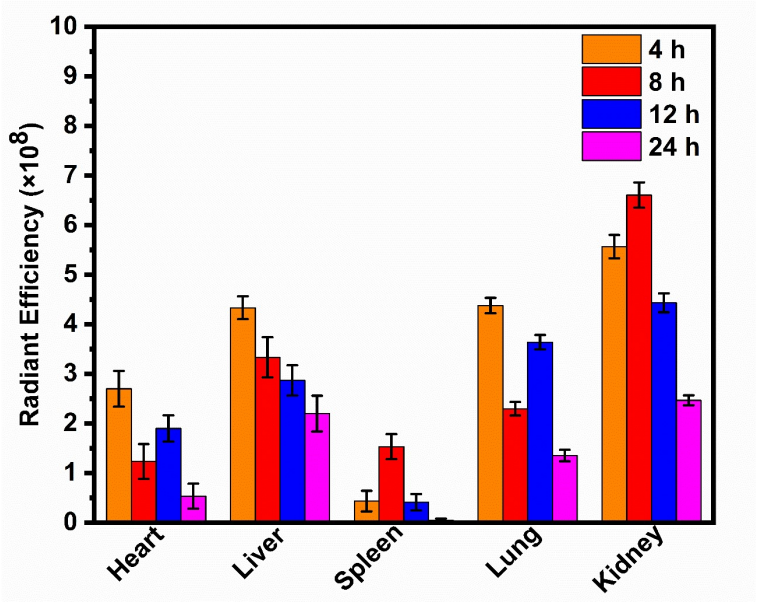

Figure S11. Cu levels in the major organs of tumor-bearing mice after intravenous injection of GPC for 4 h, 8 h, 12 h and 24 h (n=3).

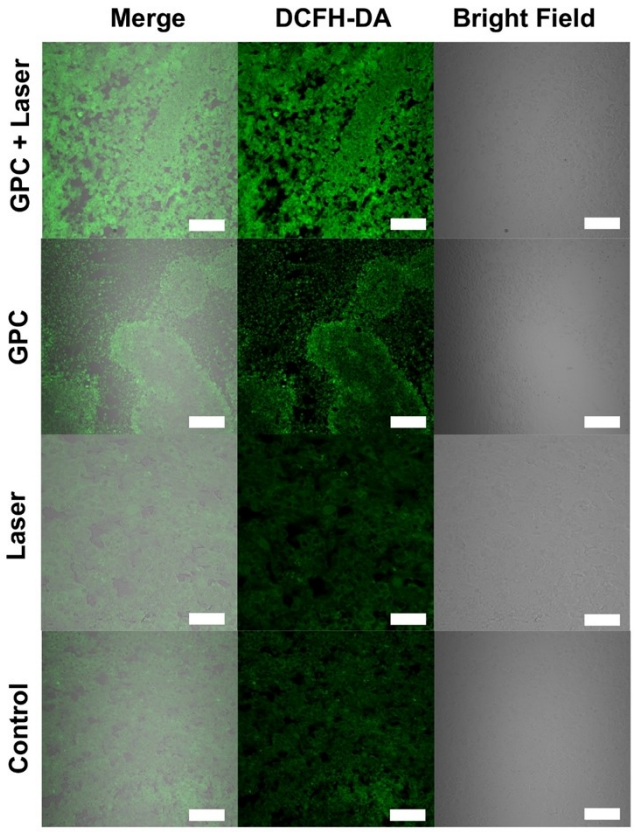

Figure S12. The levels of ROS production in tumor tissues under different treatment conditions were observed under the confocal microscopy with DCFH-DA as a fluorescent indicator.

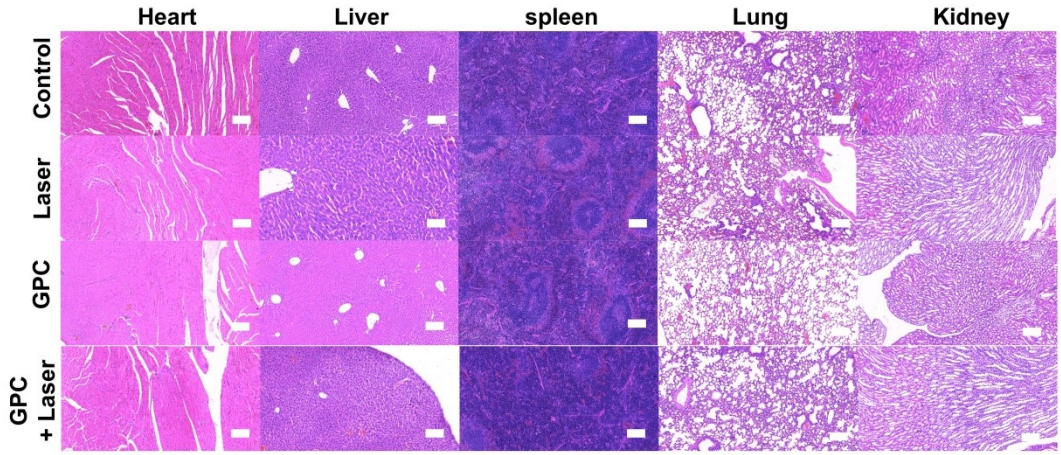

Figure S13. H&E staining of vital organ slices under different treatment conditions (bar = 100 μM).

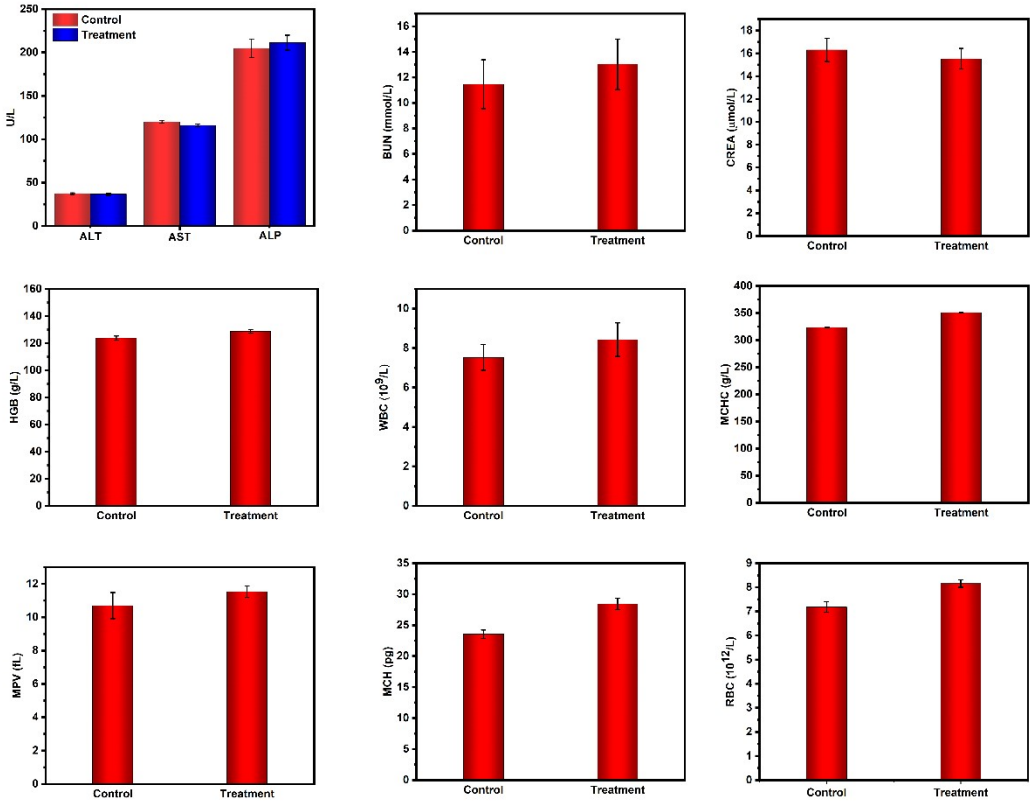

Figure S14. The serum biochemical examination of the BALB/c nude mice for three indicators: alanine aminotransferase (ALT), aspartate aminotransferase (AST), alkaline phosphatase (ALP). The blood hematological analysis for: the BUN (urea nitrogen) and serum creatinine (CREA), hemoglobin (HGB), white blood cells (WBC), mean corpuscular hemoglobin concentration (MCHC), mean platelet volume (MPV), mean corpuscular hemoglobin (MCH), Red blood cells (RBC). After intravenous injection of GPC with laser for 24 days as treatment groups, and the intravenous injection of saline as the control groups.